Mon. Not. R. astr. Soc. (1973) **163,** 163–182.

HIGH RESOLUTION OBSERVATIONS OF NEUTRAL HYDROGEN IN M33—II

The Velocity Field

P. J. Warner, M. C. H. Wright and J. E. Baldwin

(Received 1973 February 21)

SUMMARY

The radial velocity field of H I in M33 is used to derive a rotation curve out to a radius of 6 kpc and to demonstrate that large scale deviations from circular motion within 4 kpc of the nucleus are less than 3 km s^{-1}. The overall agreement between the present H I and earlier Hα radial velocities is satisfactory. A model of the distribution of mass indicates that all present data are consistent with a mass-to-light ratio of 5, almost independent of radius in the galaxy, a total mass M out to 6 kpc of $0{\cdot}92 \times 10^{10}\ M_{\odot}$ and a ratio $M_{\rm HI}/M$ of 0·10 within this radius. The thickness of the H I layer in the disk increases from 300 pc near the nucleus to 800 pc in the outer parts. A search for motions associated with a possible large scale density wave in the H I failed to detect any with an amplitude greater than 3 km s^{-1}.

1. INTRODUCTION

Previous work on the radial velocity field in M33 has enabled the overall features of the rotation curve and mass distribution to be determined. For many of the observations no more detailed analysis was possible, since the optical spectroscopy of Mayall & Aller (1942) and Brandt (1965) was restricted to relatively few points in the galaxy and the 21-cm hydrogen line observations of Volders (1959), Dieter (1962), Gordon (1971), de Jager & Davies (1971) and Huchtmeier (1973) were limited by their relatively large beam widths. Only in the Hα interferometric work of Carranza *et al.* (1968), with some 1048 radial velocity measurements out to a distance of 24 arcmin from the nucleus, was it possible to study detailed motions of, for instance, spiral arms. However, the hydrogen line observations made with the Cambridge Half Mile telescope by the present authors (Wright, Warner & Baldwin 1972, hereafter Paper I) have an angular resolution of $1{\cdot}5 \times 3{\cdot}0$ arcmin and a velocity resolution of 39 km s^{-1}, values which permit a more comprehensive study of the velocity field. At the assumed distance of 690 kpc and the inclination of M33, this resolution corresponds to about 600 pc × 600 pc in the plane. 690 kpc was preferred to the value used in Paper I (720 kpc).

The techniques used in the reduction of the 21-cm line radial velocity data are described in Section 2. Mean dynamical parameters for M33 are derived in Section 3 and in Section 4 a comparison is made between the Hα and 21-cm radial velocity measurements. A model of the distribution of mass is derived from the rotation curve in Section 5 and used to obtain the variation with radius of the mass-to-light ratio, the fractional mass of H I and the thickness of the H I layer. Non-circular motions and their possible association with spiral structure are discussed in Section 6.

2. REDUCTION TECHNIQUES

The reduction of several thousand simple profiles into a manageable and astronomically interesting form may be broken down into two steps; first one must obtain an adequate description of each profile in terms of a heliocentric radial velocity, velocity dispersion and peak brightness, and then these values must be combined to describe the dynamics of the galaxy as a whole.

The primary data are line profiles, sampled at intervals in frequency corresponding to 26 km s^{-1}. A particular profile is interpolated to give samples at intervals of 13 km s^{-1}. For an instrumental profile of half-width 39 km s^{-1}, one of these samples then has a value within 2 per cent of the peak value of the line profile. The zero level of the profile is obtained by the iterative procedure of averaging all points on the profile lying within some standard interval, say twice the rms noise level, of an assumed zero. This average is then taken as the assumed zero for the next iteration. The process provides an estimate of the continuum radiation and corrects the velocity dispersion and peak brightness for its effects. The velocities at which the profile has fallen to half the peak height are obtained: the mean of these values is used to characterize the radial velocity of the H I in the profile, and their difference, the velocity dispersion.

For the present results the H I distribution is essentially a continuous function of position, so the velocities and dispersions were combined to produce maps. The extent to which these maps represent the true velocity field depends upon two factors:

(a) *Noise on the line profiles*

The accuracy with which the mean velocity V, and the width w, of the profile between half-intensity point can be determined for an individual profile depends on the ratio of the peak brightness in the profile S to the rms noise level N and on the width, w. Using the technique described above, the rms error in the mean velocity is given by

$$(\overline{\Delta V^2})^{1/2} = \frac{w}{2{\cdot}15\,(S/N)}$$

and the rms error in the observed dispersion (uncorrected for instrumental width) by

$$(\overline{\Delta w^2})^{1/2} = \frac{w}{2{\cdot}4\,(S/N)}.$$

These results are only 10 per cent worse than those attainable using optimum filtering methods and this technique is far simpler to apply, particularly in the present case where the ' true ' width of the profile is not known in advance.

(b) *Beam smoothing*

Features of the velocity field much smaller than the beam size cannot be reproduced. The effects of gradients of projected H I density σ and of radial velocity V_{obs} across the beam are discussed in Appendix I. It is shown there that only in situations where the gradient of σ has a component parallel to the gradient of V_{obs} or where the gradient of V_{obs} changes across the beam does V_{obs} differ from the true radial velocity at the beam centre. For the present observations the former case gives rise to errors in V_{obs} which are usually less than 2 km s^{-1} and

have a maximum value of ~ 10 km s^{-1}. The effect of changes in the gradient of V_{obs} across the beam are important only within 5 arcmin of the nucleus where they may reach as much as 10 km s^{-1}. The rotation curve is in any case poorly determined in this region.

Measurements of the line-of-sight component of velocity do not permit a unique interpretation of the velocity field. The simplification usually made is to consider the galaxy as a thin inclined plane with rotation dominating over expansion or motions perpendicular to the plane. The velocity field may then be characterized by the following dynamical parameters:

1. The position of the centre of rotation.
2. V_{sys}, the systemic velocity (defined as the mean radial velocity of all points within a specified radius in the plane of the galaxy).
3. i, the inclination of the normal to the plane to the line of sight.
4. The position angle (PA) of the major axis.
5. A rotation curve $V(R)$, where R is the radial distance in the plane of the galaxy from the rotation centre.

The observed radial velocity V_{obs} is then given by

$$V_{obs} = V_{sys} + V(R) \cos\theta \sin i \tag{1}$$

where θ is the azimuthal coordinate in the plane of the galaxy measured from the major axis. Further terms may be added to describe expansion in the plane and motion normal to the galactic plane.

We now discuss the technique used for deriving a mean rotation curve from the whole velocity field and values for the other dynamical parameters. Likely values were first assumed for i, PA, V_{sys} and the position of the rotation centre. The (R, θ) coordinates in this assumed plane were calculated for each sample point in the sky. Equation (1) was then used to give the circular velocity from V_{obs}. The weighted mean of the velocities of all points lying in an annulus in the plane of the galaxy of width $2dR$ at radius R,

$$V(R) = \frac{1}{\sin i} \frac{\sum_{\theta} \sum_{R-dR}^{R+dR} \{W(R,\theta)|\cos\theta|(V_{obs}(R,\theta) - V_{sys})/\cos\theta\}}{\sum_{\theta} \sum_{R-dR}^{R+dR} W(R,\theta)|\cos\theta|} \tag{2}$$

was taken as the best measure of the circular velocity at radius R.

The weighting has two components, the first, W, proportional to the signal to noise ratio, S/N, of the profile, the second proportional to the line-of-sight component of the circular velocity. Thus velocities from profiles on the minor axis or with signal to noise ratio less than ~ 1, make no contribution to the average. The term 'rotation curve' as used hereafter will refer to the smooth curve drawn through the calculated points $V(R)$. In practice the interval $2\,dR$ was made smaller than the synthesized beam so this curve is the true rotation curve smoothed by the beam if non-circular motions are absent.

The rms deviations of the mean, $\Delta V(R)$, were also calculated for each interval of R. The weighted sum of these deviations was minimized to obtain a best fit by calculating:

$$G = \frac{\sum_{R=0}^{R_{max}} \{\sum^{\theta} W(R, \theta)|\cos\theta|\}\,\Delta V^2(R)}{\sum_{R=0}^{R_{max}} \sum^{\theta} W(R, \theta)|\cos\theta|} \qquad (3)$$

for each of a range of values of PA and i, with a fixed rotation centre and systemic velocity. The best fit values of PA and i, with errors, were found from a map of G plotted against PA and i. Small variations of systemic velocity and rotation centre were then used to improve the fit at this minimum.

The parameters obtained by this procedure were used to generate a model radial velocity distribution using equation (1) for the same grid of points as the observations. A map of this velocity field may then be compared with the observed radial velocity field. We shall call the map obtained by subtracting the model from the observed field the *residual radial velocity field.*

3. THE RESULTS

The observations are presented at two angular resolutions. In this section they will be interpreted in terms of pure circular motions.

(a) *Low resolution results*

Maps made from 20 interferometer spacings, giving a resolution of $4{\cdot}5 \times 9$ arcmin (1·8 kpc), were used to study the overall dynamics at low resolution. With a beam of this size, all profiles have good signal-to-noise ratio and define an unbroken and continuous velocity field. In the outer parts of M33 where H I surface densities are low, the rotation curve changes only slowly with radius so that little information is lost by beam smoothing: near the nucleus, however, this effect is very important.

The low resolution radial velocity field is shown in Fig. 1(a). The dashed contour shows the extent of data from profiles with $S/N > 3$ and a cross marks the optical nucleus. The overall symmetry of the pattern is that expected for circular motions of H I in an inclined plane, with differential rotation extending into the centre. However, the major axis appears to bend smoothly to smaller PA in the extreme north and south, a deviation from pure circular motion particularly noticeable at distances of more than 4 kpc from the nucleus.

The searching procedure, described in Section 2, was used on all observed radial velocities within 7·5 kpc of the nucleus. The position of best fit was:

PA	$22^\circ \pm 1^\circ$
i	$54^\circ \pm 3^\circ$
V_{sys}	-180 ± 1 km s^{-1} (heliocentric).

The quoted errors are not formally defined but are derived from the width of the minimum in G. These parameters agree well with previous determinations (Gordon 1971; de Jager & Davies 1971) at somewhat lower resolution.

The same parameters were used to generate the residual radial velocity map shown in Fig. 1(b). The residuals are larger in areas of poorer S/N as would be expected from the fitting procedure, but their consistent sign and magnitude (> 5 km s^{-1}) shows them to be real departures from the circular motion implied by the rotation curve. A discussion of their possible origin is postponed until Section 6.

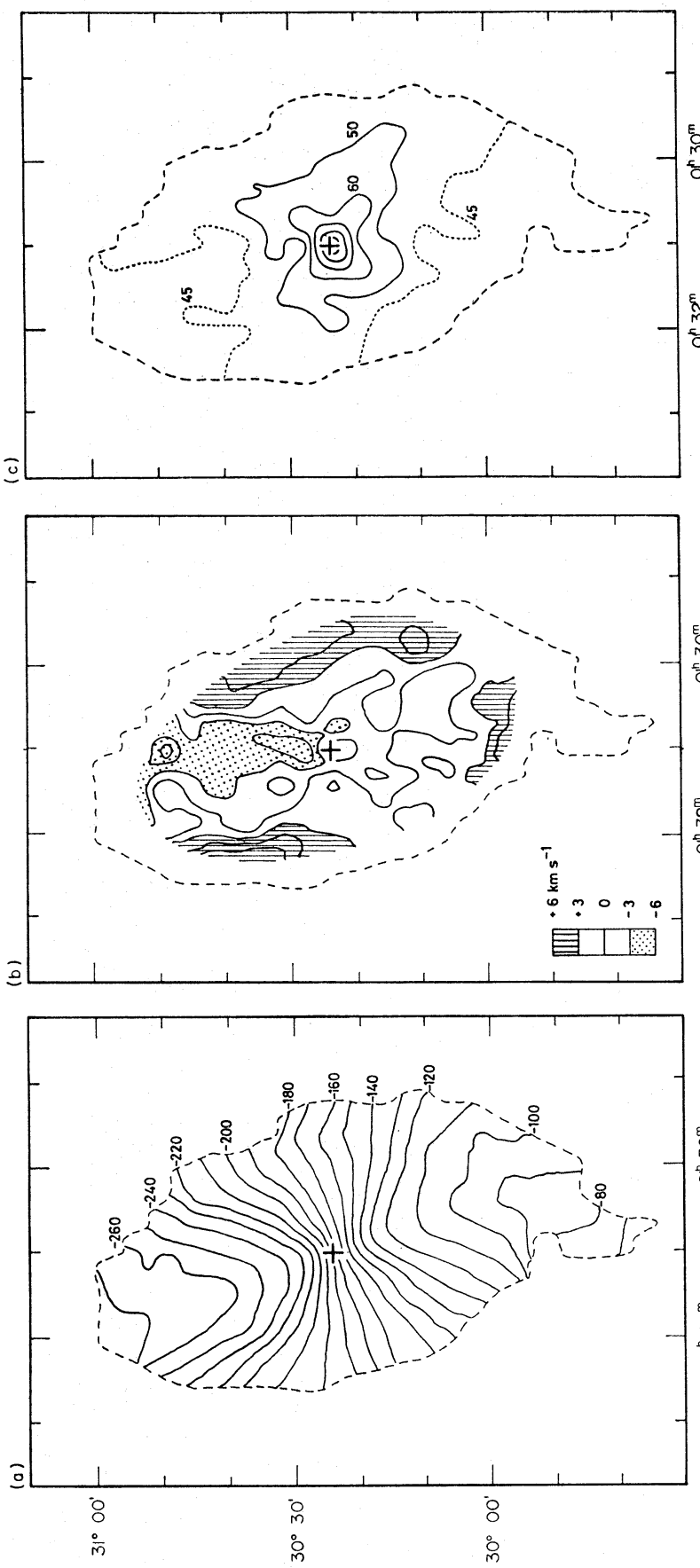

FIG. 1. *The velocity field of M33 observed with a resolution of 4′·5 × 9′·0 (a) Observed radial velocity field. The contour interval is* 10 *km s*$^{-1}$. *(b) Residual radial velocity field. The contour interval is* 3 *km s*$^{-1}$. *(c) Dispersion in radial velocity. The values plotted are the observed width of the profile between half-intensity points. The contour interval is* 10 *km s*$^{-1}$.

Fig. 1(c) shows the map of the dispersion in radial velocity, i.e. the width between half-brightness points of the observed profiles. The prominent maximum at the nucleus is due to beam smoothing of the steep velocity gradient there. In the outer parts, where beam smoothing of the rotation curve could broaden the profile by only ~ 1 km s^{-1}, the minimum value is about 45 km s^{-1} corresponding to a true width at half intensity of ~ 22 km s^{-1}.

(b) *High resolution results*

Profiles within 6 kpc of the nucleus were used to study the dynamics at high resolution. With a beam of $1{\cdot}5 \times 3{\cdot}0$ arcmin, the nucleus is significantly removed from the map centre ($\alpha = 01^h\,31^m\,00^s$, $\delta\ 30^\circ\ 24'$). Measurement of a photograph obtained with the 200-in. Hale telescope using *Smithsonian Catalogue* positions for nearby field stars, gave the position of the nucleus as $\alpha = 01^h\,31^m\,01^s{\cdot}2$, $\delta = 30^\circ\ 24'\ 27''$ (1950·0). This is the position implied by all subsequent references to the nucleus, and is the position of the cross on all relevant maps. The high resolution radial velocity field is shown in Fig. 2. The dashed outline shows the extent of regions with signal-to-noise > 2; in small areas where the signal-to-noise falls below 2 the contours are dotted. The velocity field shows considerable fine

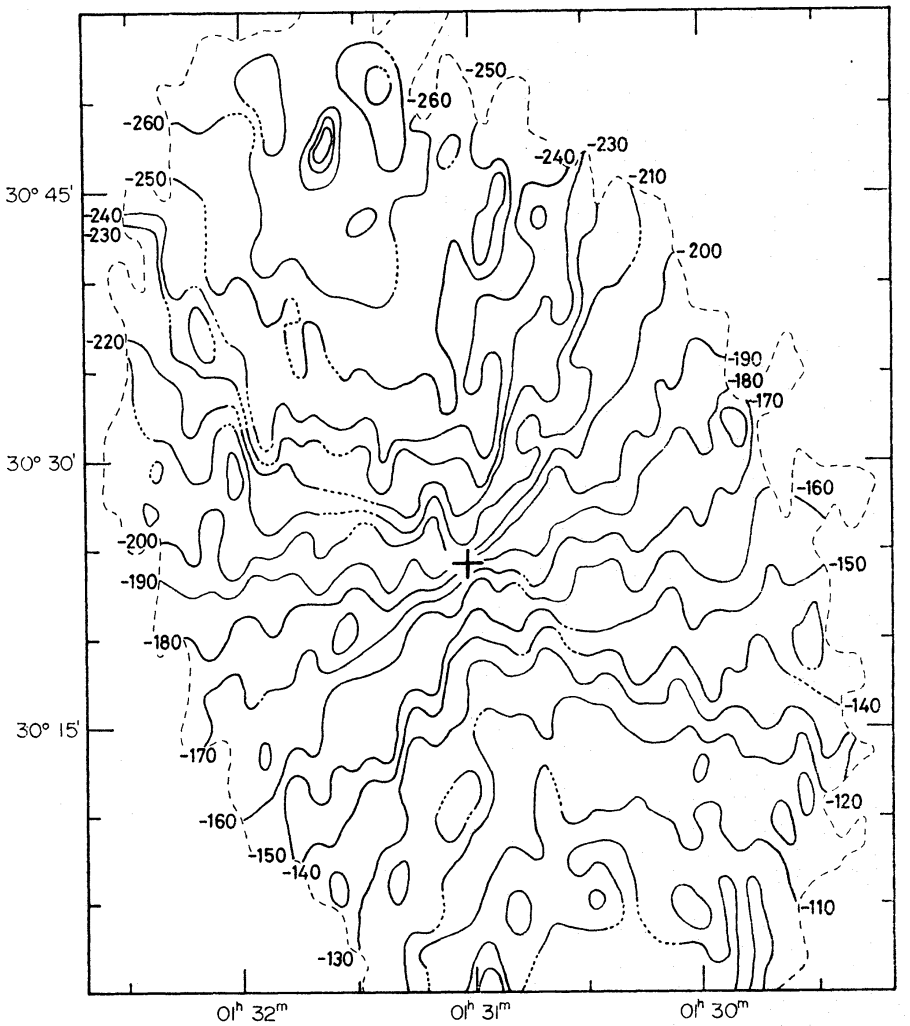

FIG. 2. *The observed radial velocity field at a resolution of* $1'{\cdot}5 \times 3'{\cdot}0$. *The contour interval is* 10 *km s*$^{-1}$*; uncertain portions are shown dotted.*

structure of ~ 10 km s^{-1} on the scale of the beam. Differential rotation extends right into the nucleus and any region of solid body rotation must be beam-sized or smaller, i.e. $\lesssim 300$ pc in radius.

The fitting procedure, when used on points within 6 kpc of the nucleus, gave best fit values of:

PA	$22° \pm 1°$
i	$52° \pm 3°$
V_{sys}	-180 ± 1 km s^{-1} (heliocentric)
Rotation centre	Coincident with optical nucleus to within 0·5 arcmin.

The procedure is seen to be insensitive to the exact value of the inclination. We have adopted a value of 54° after considering the present results and the value of 56° derived from the distribution of H I (Paper I).

The rotation curve (for PA = 22°, i = 54°, $V_{sys} = -180$ km s^{-1}) is shown in Fig. 3(a) and the values are recorded in Table I.

TABLE I

R [kpc]	$V(R)$ [km s^{-1}]	$\Omega(R)$ [km s^{-1} kpc^{-1}]	$K(R)$ [km s^{-1} kpc^{-1}]	$\Omega - K/2$ [km s^{-1} kpc^{-1}]	$\Omega + K/2$ [km s^{-1} kpc^{-1}]
0·1	19·5	195·1	—	—	—
0·3	35·4	117·7	203·7	15·9	219·6
0·5	42·9	85·8	135·1	18·3	153·4
0·7	43·6	62·2	101·7	11·3	113·0
0·9	51·4	57·0	105·7	4·1	109·9
1·1	60·0	54·5	99·9	4·5	104·5
1·3	66·2	50·9	91·9	4·9	96·8
1·5	72·9	48·6	82·5	7·3	89·8
1·7	74·9	44·0	67·1	10·5	77·5
1·9	75·8	39·8	67·1	6·3	73·4
2·1	81·6	38·8	69·3	4·1	73·5
2·3	85·0	36·9	60·0	6·9	67·0
2·5	86·3	34·5	54·6	7·2	61·8
2·7	88·6	32·8	50·9	7·3	58·2
2·9	89·0	30·7	42·7	9·3	52·0
3·1	88·2	28·4	45·7	5·6	51·3
3·3	92·4	28·0	54·6	0·6	55·3
3·5	98·4	28·1	49·6	3·3	52·9
3·7	98·7	26·6	36·2	8·5	44·8
3·9	97·5	25·0	33·7	8·1	41·8
4·1	97·8	23·8	35·2	6·2	41·4
4·3	98·4	22·9	37·8	4·0	41·7
4·5	101·1	22·5	31·9	6·5	38·4
4·7	98·5	20·9	31·7	5·1	36·8
4·9	102·4	20·9	34·0	3·9	37·9
5·1	101·2	19·8	23·9	7·9	31·8
5·3	100·2	18·9	24·9	6·4	31·3
5·5	100·2	18·2	27·2	4·6	31·8
5·7	101·0	17·7	14·4	10·5	24·9
5·9	95·5	16·2	—	—	—

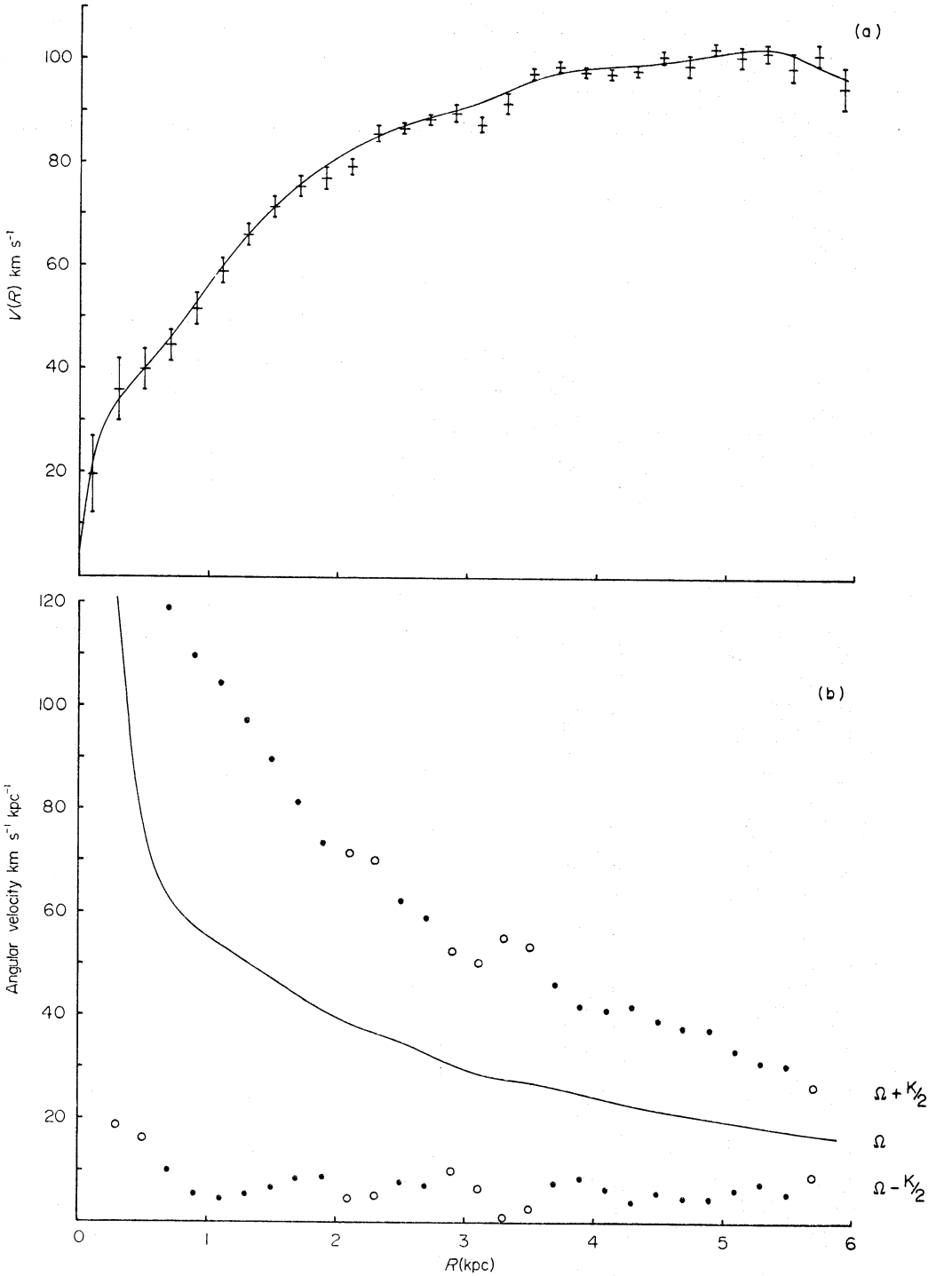

FIG. 3. (*a*) *The rotation curve of* $M33$. *The error limits shown are rms deviations of the mean.* (*b*) *The variation with radius of the angular velocity,* Ω, *and the quantities* $(\Omega \pm K/2)$. K *is the epicyclic frequency.*

The map of radial velocity dispersion is shown in Fig. 4. In some places there are profiles as broad as 80 km s^{-1}. Where these coincide with features on the radial velocity map, the large width of the profile appears to be due to an additional component having a peculiar velocity relative to the surrounding profiles. In other places broad profiles seem to be associated with regions where the mean velocity is changing rapidly with position.

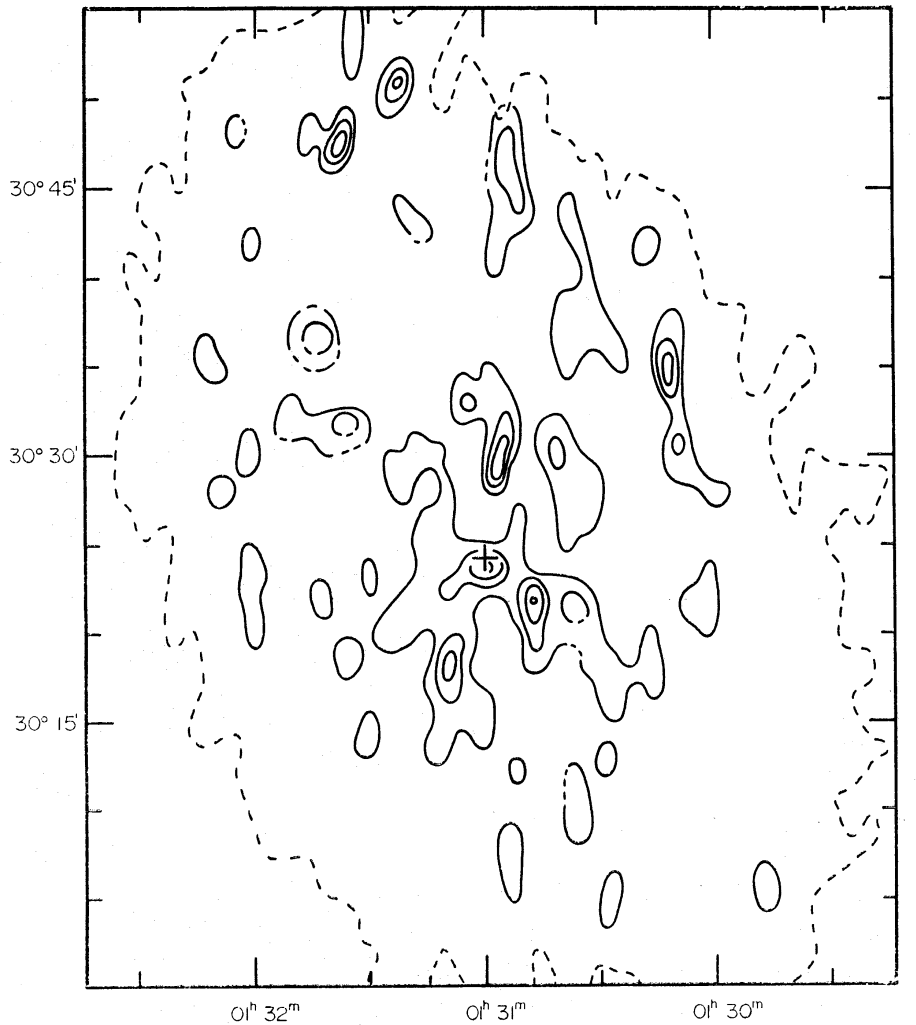

FIG. 4. *The observed dispersion w in radial velocity (i.e. the width between half-brightness points of the line profile) from observations at a resolution of* 1′·5 × 3′·6. *Contours are at* 55, 70 *and* 85 *km s*$^{-1}$.

The observed values of dispersion in radial velocity were averaged over elliptical annuli (at PA 22° and $i = 54°$) to give the variation in dispersion with radius in the disk, as shown in Fig. 5. Additional values taken from the low resolution maps are also shown at large radial distances where the effects of beam smoothing are unimportant. The lower curve in Fig. 5 shows the dispersion corrected both for the instrumental width of 39 km s^{-1} and for the comparatively small effects of beam smoothing. The corrected dispersion may be adequately represented by a linear variation with radius falling from 36 km s^{-1} near the nucleus to 22 km s^{-1} at 6 kpc. For a gaussian distribution of velocities this latter value corresponds to an rms dispersion in the line of sight of 9 km s^{-1}, very similar to the 7 km s^{-1} given by van Woerden (1967) for our Galaxy in the neighbourhood of the Sun. Our value is somewhat smaller than those of Gordon (1971) and de Jager & Davies (1971) perhaps because of the improved angular resolution.

The rotation curve has also been used to derive the variation of angular velocity, Ω and epicyclic frequency K with distance from the nucleus (where $K = 2\Omega(1+(R/2\Omega)(d\Omega/dR))^{1/2}$). The variation of Ω and $\Omega \pm K/2$ is shown in Fig. 3(b). As the value of K depends on the detailed shape of the rotation curve,

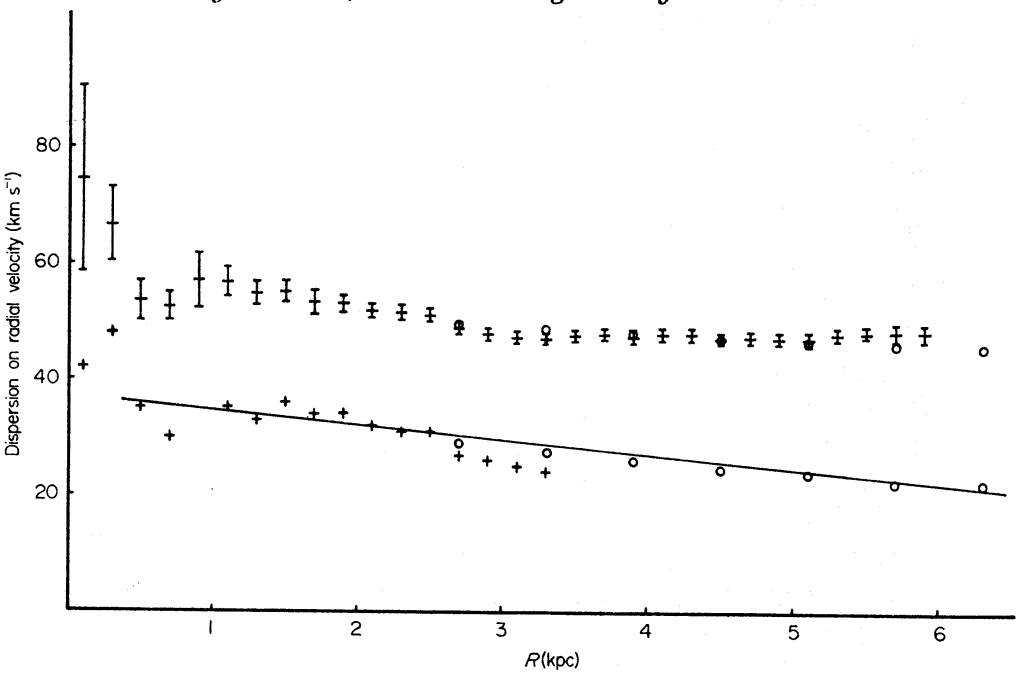

FIG. 5. *The variation with radius of the mean dispersion in radial velocity. The upper curve shows the observed width between half intensity of the profiles; the lower curve is the true width when corrected for the instrumental broadening. Circles are values from the low resolution observations.*

there are some radii where the value of $\Omega \pm K/2$ is in doubt: these values are marked by open circles in the figure.

The angular velocity $(\Omega - K/2)$ is the rate of precession of elliptical orbits of test particles making two radial oscillations per rotation period. The density variations resulting from such orbital motions also precess at the same speed. The small and near constant value of 7 km s^{-1} kpc^{-1} for $(\Omega - K/2)$ implies that such density variations would persist for many galactic rotations.

4. COMPARISON OF RADIAL VELOCITIES OF H I AND H II

The present measurements of H I radial velocities have been compared with the optical radial velocities at corresponding positions in M33 derived from two sources.

(a) The observations of bright H II regions by Mayall & Aller (1942) using the improved radial velocities obtained by Brandt (1965).

(b) The very extensive survey of radial velocities both in the arms and in the interarm regions made by Carranza *et al.* (1968).

These results are plotted in Fig. 6, together with a line of unit slope passing through the origin. We note that there is no systematic difference between the radial velocities of the H II and H I emission, even though the latter are averages over a region 1·5 × 3·0 arcmin surrounding the point at which the optical value has been measured. The scatter about the mean line is somewhat greater than that expected from the combined errors of measurement. It seems likely that this may be accounted for by the systematic motions in H II regions which are known to be 10–20 km s^{-1} in many cases and cover a range of 50 km s^{-1} in the brightest H II region in M33, NGC 604, discussed by Wright (1971). Apart from these regions where differences are to be expected, these two quite different observing techniques give radial velocities in very satisfactory agreement.

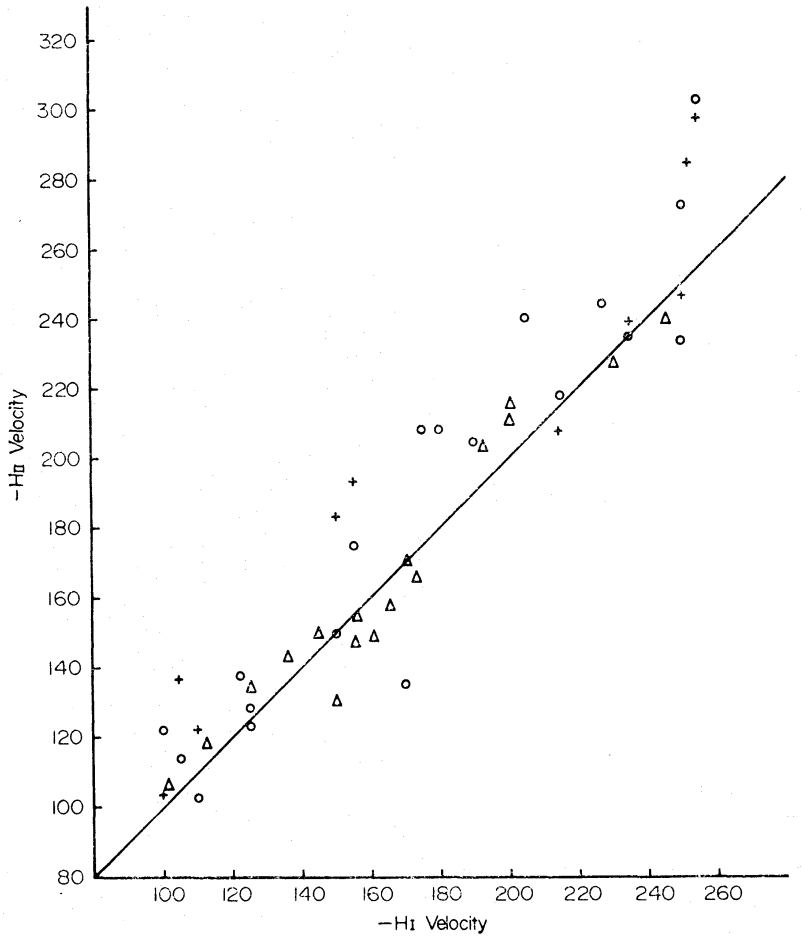

FIG. 6. *Comparison of the observed radial velocities from Hα observations with the radial velocities of the H* I *observations centred on the same points.* ○, *Brandt;* +, *de Vaucouleurs;* △, *Carranza* et al. (*averages of at least* 3 *points*).

5. THE DISTRIBUTION OF MASS

We believe that the rotation curve presented here is the most accurate obtained so far and provides a good basis for the derivation of models of the distribution of mass in M33. Several points concerning the accuracy of the curve are worth noting.

(i) The shape of the curve is only weakly dependent on the particular values chosen for the position angle and inclination of M33. The uncertainties arising from this cause are everywhere less than 2 km s^{-1}.

(ii) The rotation curve within 1 kpc of the nucleus is poorly determined from the present observations and the true slope may be greater than that shown.

(iii) Although previous authors have plotted the rotation curve for radial distances greater than 6 kpc (30 arcmin) we believe that it is misleading to do so. In Section 6 we present evidence that the material in the wings of M33 is not in circular motion in the plane defined by the main body of the galaxy. The deviation from circular motion is at least 10 km s^{-1} and makes it impossible to define the outer parts of the rotation curve with useful accuracy.

(iv) The very small departures from circular motion indicated by the map of residual velocities in Fig. 1(b) provide a sound basis for the assumption of pure circular motion within 6-kpc radius.

The model mass distributions considered were those developed by Burbidge,

Burbidge & Prendergast (1959) comprising homogeneous spheroidal shells of constant axial ratio, c/a. The rotation curve $V(R)$ was fitted by a polynomial

$$V^2(R) = \sum_{n=0}^{N} \nu_n R^n \tag{4}$$

The order of the polynomial ($N = 10$) was chosen to give a satisfactory fit to the rotation curve near the nucleus and a fairly smooth curve in the outer parts. This curve is the line shown in Fig. 3(a). The small scale feature near $R = 3$ kpc was not reproduced and indeed it is not clear whether it is part of the true rotation curve or whether it arises from some localized feature.

The density, $\rho(R)$, in the shells is related to the coefficients of the polynomial (4). The process was used to calculate as a function of radius in M33 the mass density in the plane (i.e. at $z = 0$), the surface density in the line of sight in $M_\odot$ pc^{-2} at points along the major axis, and the total mass in the model to different radii for an assumed value of the axial ratio, c/a, of the spheroids. The model believed to be most appropriate for comparison with other observations is one having an axial ratio of 0·2, for the following reason. The B photometry by de Vaucouleurs (1959) shows closely elliptical isophotes having mean observed axial ratio of 0·615. If the light distribution is assumed to be in spheroids of constant axial ratio and the inclination of 54° derived in this paper is used, then the true axial ratio of the light distribution is 0·20. The model extends to a radius of 6 kpc (30 arcmin) in the galaxy and no mass has been assigned to regions outside this spheroid. The values derived are given in Table II. As earlier workers have shown, the main effect of variations of c/a is that the derived densities are roughly inversely proportional to the axial ratio and the projected densities vary approximately as $(1 + c/a)$.

A comparison of the model with the distribution of light from B photometry (de Vaucouleurs 1959) and with the distribution of H I is also given in Table II and illustrated in Fig. 7. A striking feature of the apparent mass-to-light ratios (M/L_B) is their constancy with radius except for the values near $R = 6$ kpc which are strongly influenced by the cut-off in the model mass distribution. Most plausible extensions of the mass distribution would bring these values of (M/L) close to those at smaller radii without affecting the values for $R < 4$ kpc significantly. This result differs from the conclusions reached by Brandt (1965), Boulesteix & Monnet (1970), de Jager & Davies (1971) and Gordon (1971) who found an M/L ratio increasing with radius. The difference arises from the steeper slope of the rotation curve found at small radii with the present resolution and the rejection of the outer parts of the rotation curve as being associated with non-circular motions.

Freeman (1970), by considering infinitesimally thin disk models, suggested that the data on the disks of many spiral glaxies, including M33, are consistent with uniform mass-to-light ratios. Fitting our rotation curve to such a thin disk model we find a small increase in the mass-to-light ratio with radius. However, using the spheroidal models described above with an axial ratio of 0·2 equal to that of the light distribution, we do find a uniform mass-to-light ratio.

The total mass of the model of M33 of $0{\cdot}92 \times 10^{10} M_\odot$ out to 6-kpc radius is also appreciably lower than earlier determinations. An estimate of the thickness of the H I layer and its dependence on radius in the galaxy may be made from measures of the dispersion in radial velocity and the density at $z = 0$ in the model of the mass distribution. The velocity dispersion of the H I may be assumed to be isotropic since no large scale departures from circular motion in the disk are found

TABLE II

Physical parameters of M33

Radius R [kpc]	Projected mass and B luminosity in line of sight on major axis $[M_\odot\ pc^{-2}]$	$[L_\odot\ pc^{-2}]$	M/L_B	Projected densities in $M_\odot\ pc^{-2}$ normal to the galactic plane σ_{total}	σ_{HI}	H I layer thickness $z_{1/2}$ pc	Densities at $z = 0$ in $M_\odot\ pc^{-3}$ ρ_{HI}	ρ_{total}	ρ_{HI}/ρ_{total}
0·4	660	194	3·4	400	10·3	310	0·031	0·74	0·042
0·8	550	150	3·6	325	7·8	320	0·023	0·39	0·059
1·2	460	97	4·7	275	7·2	380	0·018	0·31	0·058
1·6	370	81	4·6	220	9·2	460	0·019	0·22	0·086
2·0	295	61	4·8	175	8·2	530	0·015	0·16	0·098
2·4	245	51	4·8	145	7·0	570	0·012	0·12	0·10
2·8	205	40	5·1	120	7·9	540	0·014	0·095	0·15
3·2	175	34	5·1	100	9·0	610	0·014	0·079	0·18
3·6	140	28	5·0	81	8·4	670	0·012	0·063	0·19
4·0	108	23	4·7	63	7·9	740	0·010	0·049	0·20
4·4	86	18	4·8	50	7·9	780	0·010	0·040	0·24
4·8	67	12	5·6	39	8·2	830	0·009	0·034	0·27
5·2	40	8·4	4·8	24	7·5	910	0·008	0·026	0·30
5·6	(14)	6·5	(2·2)	(9)	6·1	(1200)		0·014	
6·0	(0)	5·4	(0)	(0)	5·0				

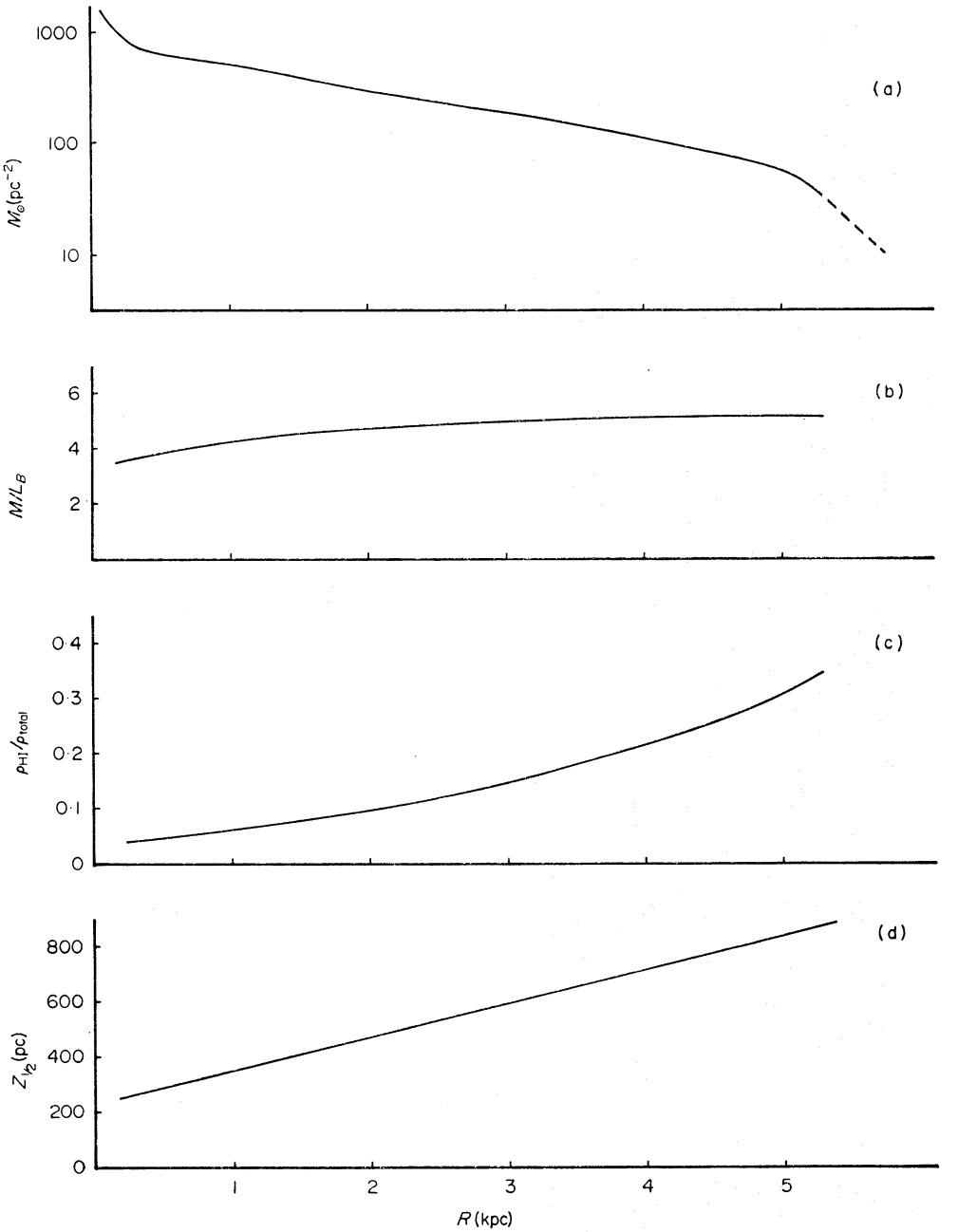

FIG. 7. *The variation with radius in the disk of M33 of physical parameters derived from the model of the distribution of mass. (a) The projected density in the line of sight at points along the major axis in $M_\odot\,pc^{-2}$. (b) The mass-to-light ratio at points along the major axis in units of $M_\odot/L_\odot$. (c) The ratio ρ_{HI}/ρ_{total} of the H I density, ρ_{HI}, to the total density, ρ_{total}. (d) The thickness $z_{1/2}$ of the H I layer between half density points.*

and differential radial motions on a small scale in the disk are likely to be rapidly damped by cloud collisions. On this assumption, the dispersion of observed radial velocity as a function of radius in the disk shown in Fig. 5 will be the same as the dispersion in the z component of velocity. The thickness, $z_{1/2}$, to half-density of the H I layer may then be deduced from the relation

$$z_{1/2} = \frac{V_{1/2}}{(2\pi\rho G)^{1/2}}$$

where both the distributions in V and z are gaussian in form and $V_{1/2}$ is the corrected width to half intensity.

The variation of thickness of the H I layer, found in this way and plotted in Fig. 7, shows a steady increase from 300 pc close to the nucleus to 800 pc at 5-kpc radius. Taking this gaussian model of the H I layer, the number density at $z = 0$ decreases from 1·0 cm^{-3} near the nucleus to 0·4 cm^{-3} at a radius of 5 kpc. These values are very similar to those found in our Galaxy.

6. NON-CIRCULAR MOTIONS

In searching for non-circular motions in M33 it is important to establish first what types of motion can be found in this analysis and what types will be concealed because they simulate the effects on the radial velocity field produced by an error in one of the dynamical parameters. This question is answered most easily by considering the radial velocity field of an ideal galaxy, in which there are only uniform circular motions in a plane, as analysed by the methods of Section 2. If all the parameters are allowed to vary, a perfect fit will be obtained, i.e. the residual velocity field will be zero everywhere. We now examine the effect of fixing one parameter at a value differing from the true one and varying the others to obtain the best fit. The residual velocity field associated with small changes in each of the dynamical parameters in turn can be derived in this way. The symmetries of the residuals are illustrated in Fig. 8; the detailed algebra is unnecessary for our

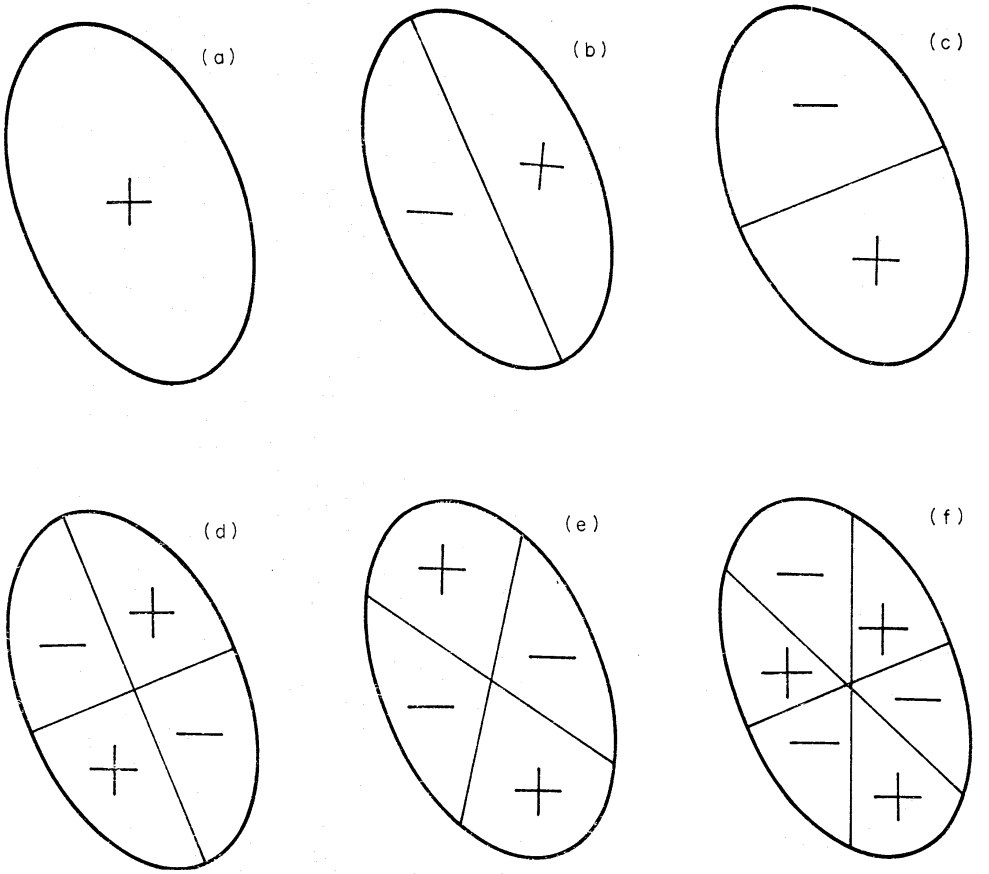

FIG. 8. *Model residual radial velocity fields corresponding to small changes in the dynamical parameters. (a) V_{sys}. (b) Position angle of major axis. (c) Rotation curve. (d) Position of rotation centre (movement along minor axis). (e) Position of rotation centre (movement along major axis). (f) Inclination.*

purpose here. The differing symmetries exhibited by these figures show firstly that the parameters fitted are essentially independent. We see also that any departure from uniform circular motion whose radial velocity field contains these symmetries will be concealed in the analysis and will appear as small deviations of the parameters from their true values.

Two types of non-circular motion which may be hard to detect are

(a) *Expansion or contraction*

The radial velocity field associated with expansion resembles that associated with changes in position angle of the major axis (Fig. 8(b)). The differences are that the latter gives a radial velocity roughly proportional to radius in the galaxy whereas expansion or contraction may be restricted to particular radial distances. Since the position angle of the major axis derived here ($22° \pm 1°$) agrees with that of the integrated hydrogen distribution ($20° \pm 2°$: Paper I) and the light distribution ($23° \pm 1°$: de Vaucouleurs 1959) to within $2°$, any concealed large scale expansion is less than 1 km s^{-1} kpc^{-1}. The residual velocity field in Fig. 1(b) shows features which might be interpreted as localized expanding motions. For instance, the features on the preceding and following edges of the galaxy would correspond to velocities of ~ 10 km s^{-1} of contraction and expansion respectively. In a region 10 arcmin north of the nucleus the residual velocities reach ~ 5 km s^{-1} corresponding to an expansion of ~ 30 km s^{-1}.

(b) *Motion of the galaxy transverse to the line of sight*

This motion is equivalent to solid body rotation of the galaxy about an axis perpendicular to the direction of transverse motion. The component in the direction of the minor axis gives a radial velocity field very similar to that in Fig. 8(b) corresponding to changes in position angle. The component in the direction of the major axis is equivalent to solid body rotation in the plane of the disk. Thus the whole of the transverse motion would be incorporated in changes in position angle and in the rotation curve.

Rotation of our Galaxy produces a gradient of the velocity field of ~ 2 km s^{-1} deg^{-1} with maximum slope at PA $\sim 100°$ for the position of M33. After correction for galactic rotation the radial velocities of members of the local group are ~ 100 km s^{-1}. Assuming these velocities to be typical of the velocities perpendicular to the line of sight, it seems unlikely that the gradient of the velocity field due to both kinds of relative motion can exceed 5 km s^{-1} deg^{-1} for M33. The most significant effect of the component of the field with gradient parallel to the major axis may well be that on the derived mass of M33. A gradient of 5 km s^{-1} deg^{-1} corresponds to a change of ~ 10 per cent in the mass. A 5 km s^{-1} deg^{-1} gradient perpendicular to the major axis of M33 would change the apparent PA of the major axis by $\sim 1°$ or correspond to linear expansion or contraction of ~ 1 km s^{-1} kpc^{-1}.

We have shown above that the observed residual velocity field (Fig. 1(b)) can be explained by contraction or expansion in localized regions. Alternatively, one may explain the positive residuals on both edges of the galaxy in the north as resulting from a larger angle of inclination, i.e. a twisting of the plane. Another possible explanation which deals qualitatively with all the residual velocities beyond $R = 4$ kpc, is that the centre of rotation of the material in the outer parts

is further north than that of material nearer the nucleus. The displacement of the rotation centre implied would be a few hundred parsecs. Such a phenomenon would be expected if the large scale distribution of mass in M33 were asymmetric.

The residual velocity field has not been plotted in the region of the wings since there are no other data at the same radii to provide an undisturbed comparison area. We note that if we interpret the radial velocities in the wings as due to circular motion in the plane of the disk, then the rotation curve rises rapidly with radius beyond 6 kpc. This feature may have led to some of the high values of total mass quoted in the past. We feel that an explanation involving departures from circular motion of only 10–20 km s^{-1} is a much more likely one.

A third type of large scale departure from circular motion is of great interest, *viz.*

(c) *Density waves*

Courtes & Dubout-Crillon (1971) and Dixon (1971) have reported evidence for the existence of a density wave in part of the southern arm of M33. We have limited ourselves to searching for motions associated with a linear density wave over the whole galaxy having the same form and phase angle as the spiral defined by the optical arms. With R, the distance from the nucleus and ϕ the phase angle of the spiral, the relation:

$$\phi[\text{degrees}] = 100 \ln\left(\frac{R[\text{kpc}]}{0{\cdot}3}\right)$$

gives an adequate description of the two-armed spiral features out to ~ 4 kpc. Following Lin, Yuan & Shu (1969) we resolves the non-circular motions into a radial component, v_R and an azimuthal one, v_θ. If this description is adequate for a spiral structure as open as that in M33, the velocity perturbation associated with the spiral pattern has the form:

$$v_R(R, \theta) = 2c(V(R) - V_p(R)) \tan(t) \sin(2\theta + \phi)$$

$$v_\theta(R, \theta) = c\left(V(R) + \frac{R\,dV}{dR}\right) \tan(t) \cos(2\theta + \phi)$$

where: c is the density contrast of the wave, i.e. max − min/max + min,
t the pitch angle of the spiral ($\tan t \sim 0{\cdot}7$ for the chosen spiral),
$V(R)$ the rotation curve,
$V_p(R)$ the pattern speed of the spiral.

The observed perturbation in radial velocity is then:

$$\delta V(R, \theta) = v_\theta(R, \theta) \cos(\theta) + v_R(R, \theta) \sin(\theta).$$

Maps of this perturbation were calculated, for a density contrast $c = \frac{1}{6}$ (Wright *et al.* 1972), using a smoothed form of the rotation curve for pattern speeds of 0, 16, 32 km s^{-1} kpc^{-1} (i.e. co-rotation at distances of infinity, 7 and 4 kpc). The 16 km s^{-1} kpc^{-1} perturbation is shown in Fig. 9. All three maps showed peculiar velocities up to 10 km s^{-1}. Their appearance was not much affected by the shape of the rotation curve but they became more complicated as the co-rotation radius was decreased.

It is clear that the radial velocity field (Fig. 9) has components having the same symmetries as some of the examples in Fig. 8. So the density-wave perturbation

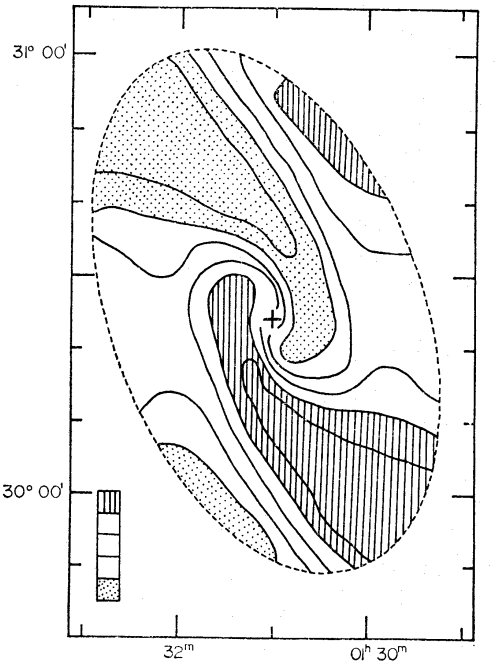

FIG. 9. *Model residual radial velocity field associated with a linear density wave in M33. For a description of the wave, see text.*

would be partially removed by the procedure for finding the best rotation curve. To test for the presence of a density-wave it is therefore necessary first to subtract the predicted velocity perturbation from the observed radial velocity field and then to fit the result as before. In all cases a worse fit was found. The north and south of the galaxy no longer had the expected symmetry, and the fitted inclinations were very low. There is little doubt that perturbations of the form and magnitude given above were not present in the galaxy as a whole.

There are, however, factors which would make the detection of such a wave difficult.

(i) The presence of other non-circular motion (z-motion or expansion) of a similar size.

(ii) An incorrect or oversimplified choice of the form of the spiral. The main spiral structure is broken and not clearly visible beyond 4 kpc; the southern arm is much better defined; more than two arms are visible.

(iii) Too high a value chosen for the density contrast c. If c were decreased to $\sim 1/20$ the maximum perturbation would be ~ 3 km s^{-1} which is near the noise level for the present observations.

7. CONCLUSIONS

The most important results of this study of the dynamics of the neutral hydrogen in M33 are:

(1) The gas motions within 4 kpc of the nucleus deviate only slightly from uniform circular motion in a plane. Beyond this distance non-circular motions become important.

(2) The mass-to-light ratio is almost independent of radial distance from the nucleus, lying in the range $4{\cdot}9 \pm 0{\cdot}3$ for radii between 0·8 and 5·2 kpc.

(3) The thickness of the H I layer between half-density points increases with radius from 300 pc near the nucleus to 800 pc in the outer parts.

(4) No systematic motions associated with a large-scale spiral density wave were found with an amplitude larger than 3 km s^{-1}.

The following table summarizes those quantities derived in this paper and in Paper I for which a single best value can be given:

Assumed distance	690 kpc
Position of optical nucleus 1950·0	$\begin{cases} 01^h\ 31^m\ 01^s.2 \\ +30^\circ\ 24'\ 27'' \end{cases}$
PA of major axis	22°
Inclination	54°
Systemic radial velocity	-180 ± 1 km s^{-1}
H I mass within 30 arcmin (6 kpc) radius	$0.90 \times 10^9\ M_\odot$
Total mass to 30 arcmin (6 kpc) radius	$0.92 \times 10^{10}\ M_\odot$
(H I mass/Total mass) within 30 arcmin	0·10
Mean M/L_B ratio	4·9

ACKNOWLEDGMENTS

We would like to thank R. Love and Mrs Anna Bullock for writing the programme used to derive the mass model and Dr J. R. Shakeshaft for his comments on the manuscript.

Mullard Radio Astronomy Observatory, Cambridge

REFERENCES

Boulesteix, J. & Monnet, G., 1970. *Astr. Astrophys.*, **9**, 350.
Brandt, J. C., 1965. *Mon. Not. R. astr. Soc.*, **129**, 309.
Burbidge, E. M., Burbidge, G. R. & Prendergast, K. H., 1959. *Astrophys. J.*, **130**, 739.
Carranza, G., Courtes, G., Georgelin, Y., Monnet, G. & Pourcelot, A., 1968. *Ann. Astrophys.* **31**, 63.
Courtes, G. & Dubout-Crillon, R., 1971. *Astr. Astrophys.*, **11**, 468.
Dieter, N. H., 1962. *Astr. J.*, **67**, 217.
Dixon, M. E., 1971. *Astrophys. J.*, **164**, 411.
Freeman, K. C., 1970. *Astrophys. J.*, **160**, 811.
Gordon, K. J., 1971. *Astrophys. J.*, **169**, 235.
Huchtmeier, W., 1973. *Astr. Astrophys.*, **22**, 91.
Jager, G. de & Davies, R. D., 1971. *Mon. Not. R. astr. Soc.*, **153**, 9.
Lin, C. C., Yuan, C. & Shu, F. H., 1969. *Astrophys. J.*, **155**, 721.
Mayall, N. U. & Aller, L. H., 1942. *Astrophys. J.*, **95**, 5.
Vaucouleurs, G. de., 1959. *Astrophys. J.*, **130**, 728.
Vaucouleurs, G. de & Vaucouleurs, A. de, 1971. *Astrophys. Lett.*, **8**, 17.
Volders, L. M. J. S., 1959. *Bull. astr. Inst. Nethl.*, **14**, 323.
Woerden, H. van, 1967. I.A.U. Symposium No. 31, *Radioastronomy and the galactic system*, p. 3. Academic Press, New York.
Wright, M. C. H., 1971. *Astrophys. Lett.*, **7**, 209.
Wright, M. C. H., Warner, P. J. & Baldwin, J. E., 1972. *Mon. Not. R. astr. Soc.*, **155**, 337.

APPENDIX I

EFFECTS OF BEAM SMOOTHING ON THE RADIAL VELOCITY FIELD

The effects of beam smoothing are most easily discussed in terms of the mean radial velocity of a line profile. This differs in general from the radial velocity as defined in Section 2 but very little for profiles that are only slightly resolved as in the present study. Let the projected density of the H I, σ, and the radial velocity, V, be written as Taylor series in terms of the values σ_0 and V_0 at the beam centre

$$\sigma = \sigma_0 + x\sigma'_x + y\sigma'_y + \tfrac{1}{2}x^2\sigma''_x + \tfrac{1}{2}y^2\sigma''_y + \ldots$$

$$V = V_0 + xV'_x + yV'_y + \tfrac{1}{2}x^2V''_x + \tfrac{1}{2}y^2V''_y + \ldots.$$

and let the beam shape $A(x, y)$ be assumed symmetrical. Then the observed mean velocity

$$\bar{V} = \frac{\iint A\sigma V\,dx\,dy}{\iint A\sigma\,dx\,dy} = \frac{\iint A\sigma_0 V_0\,dx\,dy}{\iint A\sigma_0\,dx\,dy}$$

$$\times\left\{1 + \frac{\iint A(x^2\sigma'_xV'_x + y^2\sigma'_yV_y)\,dx\,dy}{\iint A\sigma_0V_0\,dx\,dy} + \tfrac{1}{2}\frac{\iint AV_0(x^2\sigma''_x + y^2\sigma''_y)\,dx\,dy}{\iint A\sigma_0V_0\,dx\,dy}\right.$$

$$\left. + \tfrac{1}{2}\frac{\iint A\sigma_0(x^2V''_x + y^2V''_y)\,dx\,dy}{\iint A\sigma_0V_0\,dx\,dy} - \tfrac{1}{2}\frac{\iint A(x^2\sigma''_x + y^2\sigma''_y)\,dx\,dy}{\iint A\sigma_0\,dx\,dy}\right\}$$

$$\bar{V} = V_0 + \frac{\iint A(x^2\sigma'_xV'_x + y^2\sigma'_yV'_y)\,dx\,dy}{\sigma_0\iint A\,dx\,dy} + \tfrac{1}{2}\frac{\iint A(x^2V''_x + y^2V''_y)\,dx\,dy.}{\iint A\,dx\,dy}$$

Thus the only situations where the measured velocity is not that at the beam centre are those in which

(a) The gradient in σ has a component in the same direction as the gradient in V; and

(b) The gradient in V changes significantly across the beam.